ACS OMEGA

http://pubs.acs.org/journal/acsodf

Article

Spherical Sulfur-Infiltrated Carbon Cathode with a Tunable Poly(3,4-ethylenedioxythiophene) Layer for Lithium−Sulfur Batteries

Joo-Hyung Kim, Hye-Ji Eun, Su Hwan Jeong, Jihyun Jang, Mihye Wu, Jou-Hyeon Ahn, Jungdon Suk,* and San Moon*

Cite This: *ACS Omega* 2023, 8, 23799−23805

Read Online

ACCESS | Metrics & More | Article Recommendations | Supporting Information

ABSTRACT: Li−S batteries have received significant attention owing to their high energy density, nontoxicity, low cost, and eco-friendliness. However, the dissolution of lithium polysulfide during the charge/discharge process and its extremely low electron conductivity hinder practical applications of Li−S batteries. Herein, we report a sulfur-infiltrated carbon cathode material with a spherical morphology and conductive polymer coating. The material was produced via a facile polymerization process that forms a robust nanostructured layer and physically prevents the dissolution of lithium polysulfide. The thin double layer composed of carbon and poly(3,4-ethylenedioxythiophene) provides sufficient space for sulfur storage and effectively prevents the elution of polysulfide during continuous cycling, thereby playing an essential role in increasing the sulfur utilization rate and significantly improving the electrochemical performance of the battery. Sulfur-infiltrated hollow carbon spheres with a conductive polymer layer demonstrate a stable cycle life and reduced internal resistance. The as-fabricated battery demonstrated an excellent capacity of 970 mA h g^{-1} at 0.5 C and a stable cycle performance, exhibiting ∼78% of the initial discharge capacity after 50 cycles. This study provides a promising approach to significantly improve the electrochemical performance of Li−S batteries and render them as valuable and safe energy devices for large-scale energy storage systems.

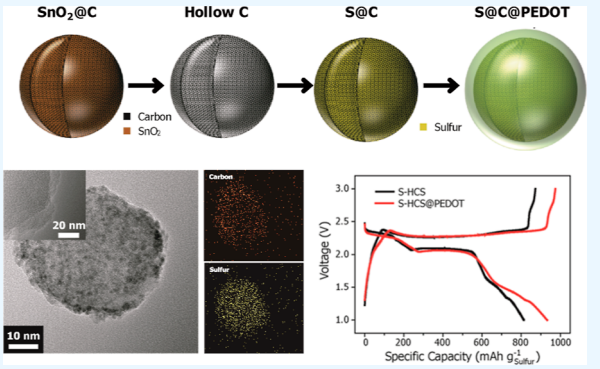

1. INTRODUCTION

The increasing use of high-performance electric vehicles, along with mobility devices and hybrid electric vehicles, has resulted in a growing demand for high-energy rechargeable storage systems.[1−7] However, current lithium-ion batteries (LIBs) cannot fully meet the energy requirements of emerging high-power devices, such as electric vehicles and unmanned aerial vehicles, because they primarily use conventional intercalation-based oxide cathode materials with limited capacities of 100−200 mA h g^{-1}.[8−10] Thus, considerable attention has been devoted to the development of alternative rechargeable battery systems with significantly improved energy densities. Among various potential systems, Li−S batteries are promising energy storage devices, which benefit from the high theoretical capacity of sulfur (1675 mA h g^{-1}), to realize a high theoretical energy density of 2500 W h kg^{-1}, which is seven times higher than that of conventional LIBs (∼387 W h kg^{-1}). Furthermore, sulfur as a cathode material has various advantages, such as nontoxicity, low cost, and abundance.[11−17]

Despite the advantages of sulfur cathodes in Li−S batteries, their application is limited by various issues, including the insulating properties of sulfur (conductivity of $\sim 10^{-30}$), large volume expansion of up to 80% when fully charged, and significant capacity loss during cycling.[18−20] In contrast to insertion-based electrodes, sulfur electrodes exhibit significant changes in structure and morphology during cycling, leading to the formation of higher-order (Li_2S_n, $2 < n \leq 8$) and lower-order lithium polysulfides (Li_2S_2 and Li_2S), which act as insulators. Furthermore, the higher-order lithium polysulfides dissolve in the liquid electrolyte during the initial discharge phase, causing a shuttling effect in which the dissolved polysulfides diffuse to the lithium anode, where they undergo reduction and then diffuse back to the sulfur cathode. As the polysulfide repeatedly cycles between the two electrodes, the active material is continuously consumed, and the lithium metal−electrolyte interface is destabilized, resulting in significant capacity reduction.[21−25] These issues need to be addressed to widen the utilization of high-energy Li−S batteries.

A promising strategy to resolve these issues is to encapsulate sulfur in a carbon-based matrix to increase the electrical

Received: April 1, 2023
Accepted: June 9, 2023
Published: June 21, 2023

ACS Publications

© 2023 The Authors. Published by American Chemical Society

conductivity of the cathode and prevent the direct dissolution of higher-order polysulfides.[26−31] Various forms of mesoporous carbon have been investigated and depending on the pore diameter, small pores (particularly nanopores) are effective in capturing higher-order polysulfides. Many studies have been conducted to predict dissolution inhibition effects due to the similar order of magnitude of the surface pore diameter of mesoporous carbon and the chain length of high-order polysulfide. However, such cathode designs could not completely mitigate the dissolution of polysulfide, as sulfur remains on the surface of mesoporous carbon, leading to the shuttling effect. Therefore, a unique structure that physically blocks the organic electrolyte but allows the passage of lithium ions should be developed to construct an ideal battery that selectively and electrochemically uses sulfur.[32−34]

In this study, we developed sulfur-infiltrated hollow carbon spheres (S-HCSs) with a conductive polymer poly(3,4-ethylenedioxythiophene) (PEDOT) coating layer (S-HCS@PEDOT). As the inner sulfur evaporates, the outer carbon layer remains intact, forming small pores in the HCS. The internal space of the HCS can store a large amount of bulk sulfur. The sulfur binds strongly to the numerous mesopores in the inner carbon layer, preventing the loss of sulfur during the charge−discharge process in a stable space, thus increasing the overall electrode loading. The thin carbon layer facilitates the diffusion of lithium ions while providing a high electrical conductivity, enabling a high battery performance. By covering the outermost carbon layer with a conductive polymer layer (PEDOT) of optimized thickness, an optimal structure that can prevent polysulfide elution can be created.[17,25,35−39] The PEDOT layer coated onto the surface of the S-HCS improves the trapping of polysulfides and serves as a buffer layer to accommodate sulfur volume changes. This electrode design can improve the electrical performance of Li−S batteries by resolving the issues of conventional electrodes.

2. RESULTS AND DISCUSSION

2.1. Physical Characterization of S-HCS@PEDOT. The key concept of the proposed electrode design is the embedded sulfur in HCS and the conductive polymer layer coating with minimal wall thickness. As schematically summarized in Figure 1, encapsulated SnO_2 in the carbon sphere was synthesized via a hydrothermal reaction (Figure 1a). First, SnO_2 was reduced to tin metal by carbon during heating at 800 °C in a high-purity N_2 atmosphere. Subsequently, HCSs with an internal carbon network structure were eventually formed (Figure 1b). As a process for synthesizing hollow carbon spheres, 2−3 nm-sized SnO_2 primary particles gather to form 70 nm-sized SnO_2@C secondary particles, and the subsequent heat treatment and etching process creates a myriad of porous structures in the carbon inner/outer shell. This provides a favorable structure for sulfur infiltration and also traps lithium polysulfide generated during the electrochemical reaction. Numerous micropores with sizes of 0.7−1.4 nm were formed in the carbon spheres, as reported earlier.[40−42] The HCS and sulfur were sequentially annealed to enhance sulfur infiltration into the micropores. The first annealing process at a lower temperature of 155 °C causes sulfur atoms to be trapped in the mesoporous surface. The second annealing process at a higher temperature of 300 °C sublimates the bulk sulfur atoms on the surface of the HCS. This process facilitates the formation of an optimized structure, in which sulfur is selectively adsorbed only on the inner surface. Subsequently, the S-HCSs were

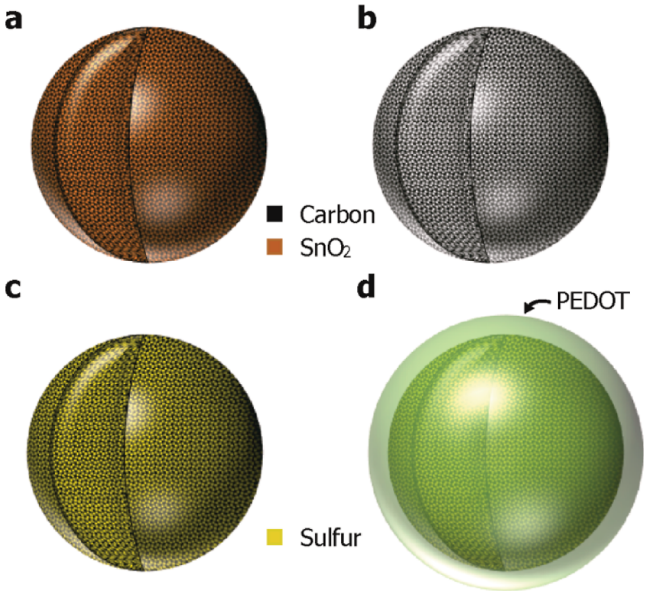

Figure 1. Schematic of S-HCS@PEDOT: (a) SnO_2@C synthesized via a hydrothermal reaction; (b) HCS; (c) S-HCS; and (d) S-HCS@PEDOT.

homogeneously coated by PEDOT. The procedure is described in detail in the Methods section, and each step in the procedure has a significant effect on the electrochemical properties of the final cell. The as-prepared SnO_2-carbon sphere is a critical structure that governs the electrochemical properties because the hollow dimensions and pore sizes are affected by the amount and size of SnO_2 particles in the carbon sphere. The ratio of the tin and carbon sources can be optimized to increase the pore dimensions and form a thin and rigid hollow carbon shell (∼2 nm), facilitating more efficient sulfur infiltration and maximizing the sulfur content. In the initial SnO_2-carbon particles, small primary particles of SnO_2 aggregate to form structures with sizes less than 5 nm, which subsequently form 50 nm secondary particles; the carbon nanolayer surrounds the surface of these secondary particles. Therefore, by controlling the amount of Sn precursor, the overall size of the final HCSs can be controlled, and the thickness of the carbon wall can be varied by controlling the amount of carbon precursor.

The carbon wall with an appropriate thickness facilitates the reaction between lithium ions and internal sulfur and helps maintain a stable morphology when internal SnO_2 is reduced during the heat treatment. Conversely, thicker carbon walls are formed when larger amounts of carbon precursors are used, resulting in smaller pore dimensions and severe damage of the carbon shell when removing Sn, as shown in Figure 2c. Because microscopic cracks in the carbon wall are inevitably generated during the reduction process, the sulfur in the micropores of the HCS come into direct contact with the electrolyte, resulting in polysulfide dissolution. Therefore, in addition to optimizing the carbon wall thickness, the dissolution of polysulfides also needs to be prevented.

Figure 3a−c shows the scanning electron microscopy (SEM) images of the carbon sphere after each step. As shown in Figure 3a,b, the morphologies of the carbon spheres with optimized carbon shells are stable, maintaining the initial particle shape without severe damage. Figure 3c shows the SEM image of S-HCS@PEDOT. Although the average particle

https://doi.org/10.1021/acsomega.3c02138
ACS Omega 2023, 8, 23799−23805

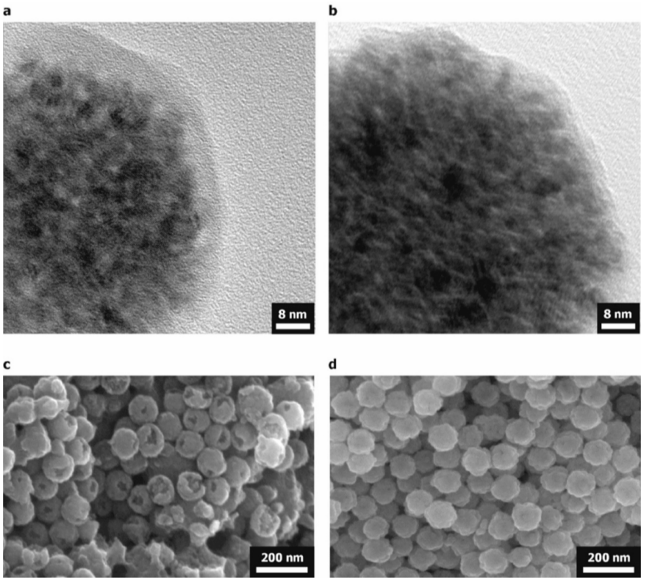

Figure 2. Morphologies of the as-synthesized SnO_2 carbon spheres and HCSs: transmission electron microscopy (TEM) images of SnO_2 carbon spheres generated from (a) large and (b) small amounts of carbon precursors. A large amount of carbon precursors increases the carbon shell thickness while decreasing the dimensions of SnO_2, which determines the pore dimensions after heat treatment. (c,d) SEM images of the HCSs corresponding to the images in (a,b), respectively.

size of S-HCS@PEDOT is similar to that of HCS, the S-HCS@PEDOT surface is significantly smoother than the HCS surface. Compared to that of HCS, the surface roughness of S-HCS@PEDOT particles is reduced. Moreover, the polymer, which covers the surface cracks caused during the earlier reductive annealing, is found between the particles and is indicated by the arrows. The inner pores and polymer layer were characterized further (Figure 3d–g) via high-resolution transmission electron microscopy (HRTEM). The HRTEM images (Figure 3d,e) show that many micropores formed at the locations where SnO_2 once existed. After the sulfur infiltration process, the pores are filled with sulfur, and the shade becomes darker, indicating the presence of sulfur (Figure 3f). As described above, the S-HCS was coated with a conductive polymer before the electrochemical tests to enhance the electrical conductivity and prevent the dissolution of polysulfides. After the polymerization of the 3,4-ethylenedioxythiophene (EDOT) monomer on the surface of the S-HCS particles, an amorphous shell of 5–10 nm in thickness forms around the S-HCS nanoparticles (Figure 3g and inset). Elemental mapping using scanning transmission electron microscopy–energy dispersive X-ray spectroscopy (STEM–EDS) was used to verify the core–shell structure of S-HCS@PEDOT (Figure 3h,i). A uniform distribution of carbon and sulfur atoms is observed, and the carbon atoms are more widely distributed than the sulfur atoms, thereby forming an outer wall. Table S1 indicates that as the PEDOT content in the electrode material increases, the absolute content of sulfur does not decrease; the relative atomic ratio changes, as determined through elemental analysis.

2.2. Surface Modification and Chemical Properties of S-HCS@PEDOT. Figure 4a shows the Fourier transform infrared (FTIR) spectra of S-HCS and S-HCS@PEDOT particles. The peaks at 1527 and 1355 cm^{-1} are attributed to

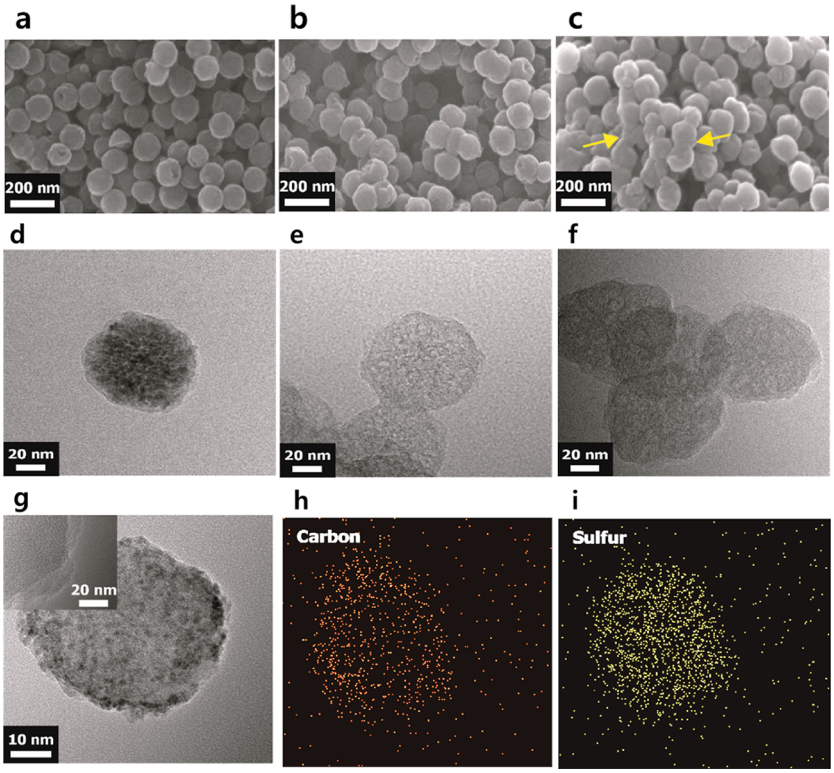

Figure 3. Characterization of S-HCS@PEDOT: SEM images of (a) HCS, (b) S-HCS, and (c) S-HCS@PEDOT. TEM images of (d) SnO_2-carbon sphere, (e) HCS, (f) S-HCS, and (g) S-HCS@PEDOT, and inset shows a higher-magnification image to clearly demonstrate the PEDOT layer. EDS elemental mapping results of (h) carbon and (i) sulfur for a single S-HCS@PEDOT particle, showing the embedded sulfur in the HCS.

https://doi.org/10.1021/acsomega.3c02138
ACS Omega 2023, 8, 23799–23805

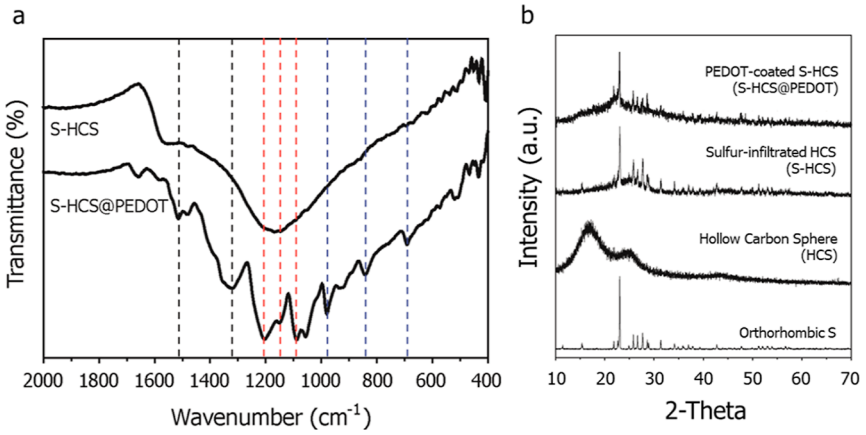

Figure 4. (a) FTIR spectra of S-HCS and S-HCS@PEDOT particles, (b) XRD patterns of pristine sulfur and as-prepared powders after each synthesis step.

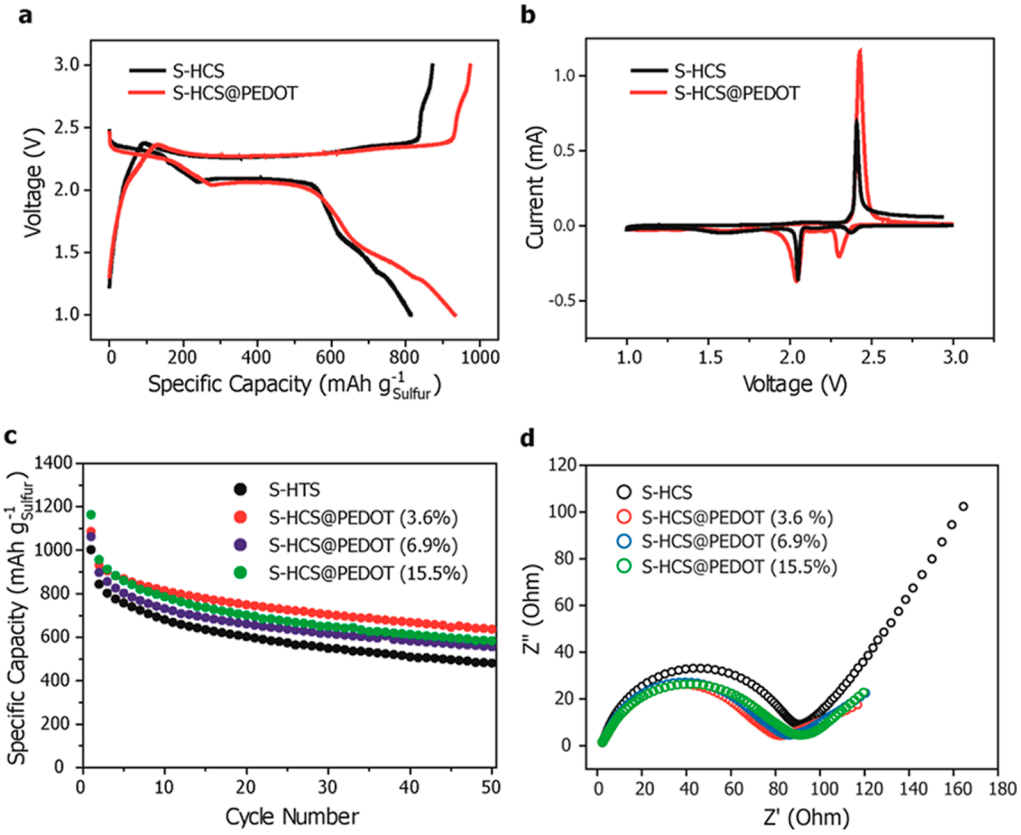

Figure 5. Electrochemical performance of the sulfur cathode: (a) galvanostatic curves of S-HCS and S-HCS@PEDOT in the second cycle at a C-rate of 0.5 C, (b) cyclic voltammograms of the cathodes at 0.1 mV s^{-1}, (c) discharge capacities of the cathode at a C-rate of 0.5 C, and (d) electrochemical impedance spectra of the cathodes.

the C═C or C−C stretching of the quinoid structure and the ring stretching of thiophene in PEDOT, respectively. The C−O−C antisymmetric stretching peaks at 1209, 1148, and 1092 cm^{-1} and the C−S vibration peaks at 987, 838, and 688 cm^{-1} originate from the ethylenedioxy group and the thiophene ring, respectively.[36] FTIR analysis confirms the existence of bonds between carbon and oxygen species, thereby indicating the successful polymerization of EDOT to form PEDOT, which is expected to afford multiple advantages, such as the complete isolation of internal sulfur and good electrical properties.

To verify the structural characteristics of the S-HCS@PEDOT nanocomposite, X-ray diffraction (XRD) analysis was conducted on the pure sulfur powder, HCSs, S-HCSs, and S-HCS@PEDOT, and the results are shown in Figure 4b. The diffraction pattern of S-HCSs exhibits orthorhombic sulfur peaks, and no crystal structure changes are observed for the S-HCS@PEDOT nanocomposite even after polymerization, although crystallinity is significantly reduced owing to the amorphous characteristics of HCSs and PEDOT.

2.3. Electrochemical Characteristics of S-HCS@PEDOT. The electrochemical performance of S-HCS@PEDOT was evaluated by measurements with coin-type half-cells. Here, 1 M lithium bis(trifluoromethanesulfonyl)imide (LiTFSI) dissolved in a cosolvent of 1,3-dioxolane and 1,2-

https://doi.org/10.1021/acsomega.3c02138
ACS Omega 2023, 8, 23799−23805

dimethoxyethane at a volume ratio of 1:1 was used as the electrolyte. Although the S-HCS shows a significantly higher discharge capacity than the ball-milled sulfur and HCS composite, issues remain such as the low cyclability of the device and the low conductivity of sulfur on the HCS surface. These drawbacks can be overcome by coating the S-HCS with conducting PEDOT layers.

To study the electrochemical characteristics of the S-HCS@PEDOT nanoparticles, the galvanostatic curves were initially determined at a C-rate of 1 C and 0.5 C, respectively (Figures 5a and S1). The typical two-plateau characteristic was observed for the sulfur cathode at 2.3 and 2.1 V, corresponding to the formation of long-chain polysulfides (Li_2S_x, $4 \leq x \leq 8$) and short-chain Li_2S_2 and Li_2S, respectively. To understand the role of hollow carbon spheres and sulfur encapsulation on the porous structure, carbon nanoparticles were mixed with sulfur and composites were prepared using a conventional heat treatment process, as shown in Figure S2a,b, respectively. The electrochemical performances of the first three cycles at 0.5 C of this composite are shown in Figure S2c, which shows a lower reversible capacity of about 600 mA h g^{-1} compared to S-HCS@PEDOT. Furthermore, cyclic voltammetry (CV) scans were performed at a scan rate of 0.1 mV s^{-1}, the results of which are shown in Figure 5b. Consistent with the voltage profiles (Figure 5a), two reductive peaks at 2.3 and 2.1 V are observed in the cyclic voltammogram. When the voltage sweep was reversed, the CV plot exhibited a peak at 2.4 V. This indicates that two oxidative peaks exist and overlap with each other, corresponding to the reverse reactions. The CV profile of the S-HCS sample in Figure 5b is represented by the black line. The redox peak exists in a similar position; however, its amplitude is lower than that of the peak observed for S-HCS@PEDOT. The reason for the small reduction peak observed at 2.4 V is that the cathode's electrochemical reaction was not uniform due to the high resistance of the sample that lacked a PEDOT coating. Additionally, it is believed that the high-order polysulfide generation reaction was not sufficient during the first discharge cycle, as shown in the CV profile of the first cycle. As a result, the reduction peak at 2 V is comparatively smaller for the sample with the PEDOT coating. In Figure 5a, the discharge capacity of the second cycle is 970 mA h g^{-1} at a current rate of 0.5 C (1 C = 1675 mA g^{-1}), which is higher than that of bare S-HCS composite because of two reasons. First, the PEDOT coating prevents the dissolution of polysulfide, enabling the conversion of more polysulfides to Li_2S, which is evidenced by a significant difference in capacity in voltage profiles below 2.1 V. Below 2.1 V, the capacity of S-HCS@PEDOT is significantly higher (~700 mA h g^{-1}) than that of S-HCS (~550 mA h g^{-1}). The solubility of newly formed high-order polysulfides decreases owing to the encapsulation by PEDOT. Second, the high electronic conductivity of PEDOT, which is used as a conductive coating, can enhance the high-rate performance of insulating materials. The electrochemical impedance spectra in Figure 5d show that R_{ct} decreases from 96 (S-HCS) to 80 Ω (S-HCS@PEDOT) after PEDOT encapsulation, which indicates that the conductive PEDOT shell facilitates electrical conduction. These findings suggest that the encapsulation of high-order polysulfides by the conductive polymer promotes electron transfer, enhances the Li^+ diffusion path, and contributes to the formation of a uniform reaction environment. In contrast, for S-HCS with exposed sulfur particles, the reduction step is limited to sites in contact with the conductive network. Moreover, high-order polysulfides may be reduced to insoluble low-order polysulfides (Li_2S_2 and Li_2S) that act as insulators near the surface, which may hinder the reduction of polysulfides away from the contact sites. This would lead to a rapid increase in the polarization of the electrode at a high C-rate.

The cycling performance, which is an important and challenging aspect of Li-ion cell operation, was also evaluated in the galvanostatic mode. The discharge capacities were measured at a C-rate of 1 C, while maintaining the charge rate at 0.5 C. As shown in Figure 5c, after 50 cycles at 1 C, the S-HCS@PEDOT cells show better capacity retention compared to the S-HCS cells. After 50 cycles, the capacity of S-HCS decreased to ~53% of its initial discharge capacity, whereas the 3.6% PEDOT-coated S-HCS retained ~78% of its initial discharge capacity. The enhanced cycling performance results from PEDOT encapsulation, which restricts the diffusion of polysulfides, thereby alleviating the self-discharging and shuttling effects. Furthermore, the PEDOT buffer layer can effectively accommodate the volume changes during the cycling process. However, for samples with higher PEDOT contents (6.9% and 15.5% PEDOT), the PEDOT coating layer was thick, which hindered electron migration or Li^+ diffusion and deteriorated the cathode performance.

3. CONCLUSIONS

We successfully fabricated a double-layered nanostructure electrode that could prevent the dissolution of lithium polysulfide, a significant issue that limits the performance of conventional Li−S batteries. The nanostructure comprised S-HCS with a PEDOT coating layer. Using our synthesis method, the thickness of the amorphous carbon−PEDOT double layer could be easily controlled. The inner carbon matrix and PEDOT layer could store large amounts of sulfur through encapsulation and provide abundant electron transport active sites, enabling the rapid transfer of electrons. Moreover, the PEDOT layer served as a shielding layer against electrolytes which cause the dissolution of polysulfides. Owing to these structural advantages, our S-HCS@PEDOT cathode material showed excellent electrochemical properties, such as a high discharge capacity (970 mA h g^{-1}) and low electrical resistance (80 Ω). This study offers a facile and cost-effective strategy to construct three-dimensional nanostructured sulfur cathodes with a thin carbon layer and conductive polymer coating for Li−S batteries.

4. METHODS

4.1. Preparation of the HCSs. The SnO_2@C spheres were synthesized via a simple hydrothermal method, in which 4.0 g of glucose and 0.214 g of $Na_2SnO_3 \cdot H_2O$ (molar ratio of 25:1) were dissolved in 40 mL of deionized water and then stirred for 30 min. This solution was transferred to a 50 mL Teflon-lined stainless-steel autoclave and heated to 160 °C for 15 h, followed by washing with deionized water and drying at 50 °C for 24 h. The obtained SnO_2@C spheres were heated to 800 °C in a N_2 atmosphere for 12 h and then washed with 12 M HCl to remove residual Sn.[40]

4.2. Preparation of S-HCSs. The HCSs and sulfur (weight ratio of 1:3) were mixed via ball milling for 12 h. The mixture was heated to 155 °C for 12 h in a closed vessel to promote sulfur infiltration and then heated to 300 °C for 2 h in an inert atmosphere to remove any residual sulfur.

https://doi.org/10.1021/acsomega.3c02138
ACS Omega 2023, 8, 23799−23805

4.3. Preparation of the S-HCS@PEDOT Nanocomposite. The as-prepared carbon composites and $FeCl_3$ were added to 250 mL of deionized water and mixed for 2 h. The EDOT monomer was first dissolved in 10 mL of deionized water containing 0.025 g of polyvinylpyrrolidone, and the solution was then slowly added to the mixture of S-nanoparticle solution and $FeCl_3$ for polymerization. The resulting mixture was stirred for 24 h at room temperature. After polymerization, 100 mL of 1 M HCl was added, and the remaining solid was then collected and diluted with deionized water until a neutral pH was reached. The product was dried at 50 °C for 48 h under vacuum to produce the S-HCS@PEDOT nanocomposites.

4.4. Characterization. The weight fractions of carbon and sulfur were determined using an elemental analyzer (Flash 2000, Thermo Scientific). The morphologies of the materials were observed using field-emission SEM (FE-SEM, Hitachi S-4800) and field-emission transmission electron microscopy (FE-TEM, Tecnai G^2 F30 S-Twin). Energy-dispersive X-ray spectroscopy elemental mapping (Tecnai G^2 F30 S-Twin) was performed to visualize the location of each element. The XRD data were recorded on a diffractometer (Model D/MAM 2500, Rigaku Co.) using Cu Kα radiation (λ = 1.5406 Å at 40 kV and 300 mA) and were collected over a 2θ range of 10−40°.

4.5. Electrochemical Measurements of S-HCS@PEDOT. For electrochemical measurements, 2032-type coin cells (MTI Corporation) were assembled in an argon-filled glovebox. The prepared sample and lithium foil (Alfa Aesar) were used as the working and counter/reference electrodes, respectively. The typical mass loading of the active material was approximately 1.0 mg cm^{-2}. The electrolyte was prepared by dissolving 1 M LiTFSI in cosolvents of 1,3-dioxolane (anhydrous, contains ∼75 ppm butylated hydroxytoluene as an inhibitor, 99.8%, Sigma-Aldrich) and 1,2-dimethoxyethane (anhydrous, 99.5%, Sigma-Aldrich) at a volume ratio of 1:1. Before preparing the electrolyte, the solvents were placed in molecular sieves for 24 h to remove moisture. Polypropylene membranes (Celgard Inc.) were used as separators. Galvanostatic measurements were performed in the potential range of 1.0−3.0 V vs Li/Li^+ using a battery cycler (WonATech WBS3000). For the rate capability tests, the charge rate was fixed at 0.5 C in the constant-current mode, and the discharge rate was varied from 0.5 to 10 C (1 C = 1675 mA g^{-1}). CV measurements were obtained in the potential range of 1.0−3.0 V vs Li/Li^+ at a scan rate of 0.1 mV s^{-1} using a multichannel battery tester (Biologic VMP3). All electrochemical measurements were conducted at 25 °C.

■ ASSOCIATED CONTENT

Supporting Information

The Supporting Information is available free of charge at https://pubs.acs.org/doi/10.1021/acsomega.3c02138.

Galvanostatic curves of synthesized samples in the first cycle at 0.5C, SEM image and galvanostatic curves of the sulfur-mixed conventional carbon nanoparticles, and table with elemental analysis value of sulfur composites (PDF)

■ AUTHOR INFORMATION

Corresponding Authors

Jungdon Suk − *Energy Materials Research Center, Korea Research Institute of Chemical Technology, Daejeon 34114, Republic of Korea*; Email: jdsuk@krict.re.kr

San Moon − *Energy Materials Research Center, Korea Research Institute of Chemical Technology, Daejeon 34114, Republic of Korea*; Phone: +82-10-8447-0331; Email: san82@krict.re.kr

Authors

Joo-Hyung Kim − *Department of Materials Engineering and Convergence Technology, Gyeongsang National University, Jinju 52828, Republic of Korea*; orcid.org/0000-0003-4247-2850

Hye-Ji Eun − *Energy Materials Research Center, Korea Research Institute of Chemical Technology, Daejeon 34114, Republic of Korea*

Su Hwan Jeong − *Department of Materials Engineering and Convergence Technology, Gyeongsang National University, Jinju 52828, Republic of Korea*

Jihyun Jang − *Department of Chemistry, Sogang University, Seoul 04107, Republic of Korea*

Mihye Wu − *Energy Materials Research Center, Korea Research Institute of Chemical Technology, Daejeon 34114, Republic of Korea*; orcid.org/0000-0003-1068-906X

Jou-Hyeon Ahn − *Department of Materials Engineering and Convergence Technology, Gyeongsang National University, Jinju 52828, Republic of Korea*; orcid.org/0000-0003-3079-8650

Complete contact information is available at: https://pubs.acs.org/10.1021/acsomega.3c02138

Notes

The authors declare no competing financial interest.

■ ACKNOWLEDGMENTS

This research was supported by project no. SS2222-20 funded by Korea Research Institute of Chemical Technology (KRICT) and Technology innovation Program (20011173) funded by the Ministry of Trade, Industry, and Energy (MOTIE), Republic of Korea. This study was also supported through a grant from the National Research Foundation of Korea (NRF) funded by the Korean Government (NRF-2021R1A4A1030318).

■ REFERENCES

(1) Whittingham, M. S. Lithium Batteries and Cathode Materials. *Chem. Rev.* **2004**, *35*, 4271−4301.

(2) Armand, M.; Tarascon, J. M. Building Better Batteries. *Nature* **2008**, *451*, 652−657.

(3) Goodenough, J. B.; Kim, Y. Challenges for Rechargeable Li Batteries. *Chem. Mater.* **2010**, *22*, 587−603.

(4) Scrosati, B.; Hassoun, J.; Sun, Y. K. Lithium-Ion Batteries. A Look into the Future. *Energy Environ. Sci.* **2011**, *4*, 3287−3295.

(5) Bruce, P. G.; Freunberger, S. A.; Hardwick, L. J.; Tarascon, J. M. Li-O_2 and Li-S Batteries with High Energy Storage. *Nat. Mater.* **2011**, *11*, 19−29.

(6) Manthiram, A.; Fu, Y. Z.; Chung, S. H.; Zu, C. X.; Su, Y. S. Rechargeable Lithium-Sulfur Batteries. *Chem. Rev.* **2014**, *114*, 11751−11787.

(7) Chung, S. H.; Manthiram, A. Current Status and Future Prospects of Metal-Sulfur Batteries. *Adv. Mater.* **2019**, *31*, No. e1901125.

(8) Manthiram, A. Materials Challenges and Opportunities of Lithium Ion Batteries. *J. Phys. Chem. Lett.* **2011**, *2*, 176−184.
(9) Larcher, D.; Tarascon, J. M. Towards Greener and More Sustainable Batteries for Electrical Energy Storage. *Nat. Chem.* **2015**, *7*, 19−29.
(10) Choi, J. W.; Aurbach, D. Promise and Reality of Post-lithium-Ion Batteries with High Energy Densities. *Nat. Rev. Mater.* **2016**, *1*, 16013.
(11) Yang, Y.; Zheng, G. Y.; Cui, Y. Nanostructured Sulfur Cathodes. *Chem. Soc. Rev.* **2013**, *42*, 3018−3032.
(12) Seh, Z. W.; Sun, Y. M.; Zhang, Q. F.; Cui, Y. Designing High-Energy Lithium-Sulfur Batteries. *Chem. Soc. Rev.* **2016**, *45*, 5605−5634.
(13) Li, G. R.; Wang, S.; Zhang, Y. N.; Li, M.; Chen, Z. W.; Lu, J. Revisiting the Role of Polysulfides in Lithium-Sulfur Batteries. *Adv. Mater.* **2018**, *30*, No. e1705590.
(14) Fan, L. L.; Li, M.; Li, X. F.; Xiao, W.; Chen, Z. W.; Lu, J. Interlayer Material Selection for Lithium-Sulfur Batteries. *Joule* **2019**, *3*, 361−386.
(15) Ji, X. L.; Nazar, L. F. Advances in Li-S Batteries. *J. Mater. Chem.* **2010**, *20*, 9821−9826.
(16) Ahad, S. A.; Kumar, P. R.; Kim, J. H.; Kim, D. J.; Ragupathy, P.; Kim, D. K. Catecholamine-Functionalized Reduced Graphene Oxide: A Scalable Carbon Host for Stable Cycling in Lithium−Sulfur Batteries. *Electrochim. Acta* **2017**, *246*, 451−458.
(17) Moon, S.; Yoo, J. K.; Jung, Y. H.; Kim, J. H.; Jung, Y. S.; Kim, D. K. Effective Suppression of Polysulfide Dissolution by Uniformly Transfer-Printed Conducting Polymer on Sulfur Cathode for Li-S Batteries. *J. Electrochem. Soc.* **2017**, *164*, A6417−A6421.
(18) Liang, C. D.; Dudney, N. J.; Howe, J. Y. Hierarchically Structured Sulfur/Carbon Nanocomposite Material for High-Energy Lithium Battery. *Chem. Mater.* **2009**, *21*, 4724−4730.
(19) Wu, F.; Chen, J. Z.; Chen, R. J.; Wu, S. X.; Li, L.; Chen, S.; Zhao, T. Sulfur/Polythiophene with a Core/Shell Structure: Synthesis and Electrochemical Properties of the Cathode for Rechargeable Lithium Batteries. *J. Phys. Chem. C* **2011**, *115*, 6057−6063.
(20) Xin, S.; Gu, L.; Zhao, N. H.; Yin, Y. X.; Zhou, L. J.; Guo, Y. G.; Wan, L. J. Smaller Sulfur Molecules Promise Better Lithium-Sulfur Batteries. *J. Am. Chem. Soc.* **2012**, *134*, 18510−18513.
(21) Yamin, H.; Gorenshtein, A.; Penciner, J.; Sternberg, Y.; Peled, E. Lithium Sulfur Battery: Oxidation/Reduction Mechanisms of Polysulfides in THF Solutions. *J. Electrochem. Soc.* **1988**, *135*, 1045−1048.
(22) Aurbach, D.; Pollak, E.; Elazari, R.; Salitra, G.; Kelley, C. S.; Affinito, J. On the Surface Chemical Aspects of Very High Energy Density, Rechargeable Li-Sulfur Batteries. *J. Electrochem. Soc.* **2009**, *156*, A694−A702.
(23) Suo, L.; Hu, Y. S.; Li, H.; Armand, M.; Chen, L. A New Class of Solvent-in-Salt Electrolyte for High-Energy Rechargeable Metallic Lithium Batteries. *Nat. Commun.* **2013**, *4*, 1481.
(24) Yun, J. H.; Kim, J. H.; Kim, D. K.; Lee, H. W. Suppressing Polysulfide Dissolution via Cohesive Forces by Interwoven Carbon Nanofibers for High-Areal-Capacity Lithium-Sulfur Batteries. *Nano Lett.* **2018**, *18*, 475−481.
(25) Han, P.; Chung, S. H.; Manthiram, A. Designing a High-Loading Sulfur Cathode with a Mixed Ionic-Electronic Conducting Polymer for Electrochemically Stable Lithium-Sulfur Batteries. *Energy Storage Mater.* **2019**, *17*, 317−324.
(26) Ji, X.; Lee, K. T.; Nazar, L. F. A Highly Ordered Nanostructured Carbon-Sulphur Cathode for Lithium-Sulphur Batteries. *Nat. Mater.* **2009**, *8*, 500−506.
(27) Wang, H. L.; Yang, Y.; Liang, Y. Y.; Robinson, J. T.; Li, Y. G.; Jackson, A.; Cui, Y.; Dai, H. J. Graphene-Wrapped Sulfur Particles as a Rechargeable Lithium-Sulfur Battery Cathode Material with High Capacity and Cycling Stability. *Nano Lett.* **2011**, *11*, 2644−2647.
(28) Moon, S.; Jung, Y. H.; Jung, W. K.; Jung, D. S.; Choi, J. W.; Kim, D. K. Encapsulated Monoclinic Sulfur for Stable Cycling of Li-S Rechargeable Batteries. *Adv. Mater.* **2013**, *25*, 6547−6553.
(29) Fu, Y. Z.; Su, Y. S.; Manthiram, A. Li_2S-Carbon Sandwiched Electrodes with Superior Performance for Lithium-Sulfur Batteries. *Adv. Energy Mater.* **2014**, *4*, 1300655.
(30) Kim, J. H.; Jung, Y. H.; Yun, J. H.; Ragupathy, P.; Kim, D. K. Enhancing the Sequential Conversion-Alloying Reaction of Mixed Sn-S Hybrid Anode for Efficient Sodium Storage by a Carbon Healed Graphene Oxide. *Small* **2018**, *14*, 1702605.
(31) Yun, J. H.; Kim, J. H.; Ragupathy, P.; Kim, D. J.; Kim, D. K. Functional and Structural Insight into Lignocellulosic Fibers for High-Areal-Capacity Lithium-Sulfur Batteries. *J. Mater. Chem. A* **2021**, *9*, 18260−18271.
(32) Kim, J. H.; Yun, J. H.; Kim, D. K. A Robust Approach for Efficient Sodium Storage of GeS_2 Hybrid Anode by Electrochemically Driven Amorphization. *Adv. Energy Mater.* **2018**, *8*, 1703499.
(33) Moorthy, B.; Kwon, S.; Kim, J. H.; Ragupathy, P.; Lee, H. M.; Kim, D. K. Tin Sulfide Modified Separator as an Efficient Polysulfide Trapper for Stable Cycling Performance in Li-S Batteries. *Nanoscale Horiz.* **2019**, *4*, 214−222.
(34) Saroha, R.; Heo, J.; Li, X.; Angulakshmi, N.; Lee, Y.; Ahn, H. J.; Ahn, J. H.; Kim, J. H. Asymmetric Separator Integrated with Ferroelectric-BaTiO3 and Mesoporous-CNT for the Reutilization of Soluble Polysulfide in Lithium-Sulfur Batteries. *J. Alloys Compd.* **2022**, *893*, 162272.
(35) Hassoun, J.; Scrosati, B. A High-Performance Polymer Tin Sulfur Lithium Ion Battery. *Angew. Chem., Int. Ed. Engl.* **2010**, *49*, 2371−2374.
(36) Shin, H. J.; Jeon, S. S.; Im, S. S. CNT/PEDOT Core/Shell Nanostructures as a Counter Electrode for Dye-Sensitized Solar Cells. *Synth. Met.* **2011**, *161*, 1284−1288.
(37) Liu, B. R.; Bo, R. H.; Taheri, M.; Di Bernardo, I.; Motta, N.; Chen, H. J.; Tsuzuki, T.; Yu, G. H.; Tricoli, A. Metal−Organic Frameworks/Conducting Polymer Hydrogel Integrated Three-Dimensional Free-standing Monoliths as Ultrahigh Loading Li-S Battery Electrodes. *Nano Lett.* **2019**, *19*, 4391−4399.
(38) Gueon, D.; Kim, T.; Lee, J.; Moon, J. H. Exploring the Janus structure to improve kinetics in sulfur conversion of Li-S batteries. *Nano Energy* **2022**, *95*, 106980.
(39) Kim, K.; Kim, J.; Moon, J. H. The Polysulfide-Cathode Binding Energy Landscape for Lithium Sulfide Growth in Lithium-Sulfur Batteries. *Adv. Sci.* **2023**, *10*, 2206057.
(40) Hu, Z.; Yan, Z.; Shen, P. K.; Zhong, C. J. Nano-Architectures of Ordered Hollow Carbon Spheres Filled with Carbon Webs by Template-Free Controllable Synthesis. *Nanotechnology* **2012**, *23*, 485404.
(41) Zhou, W.; Hu, X.; Bai, X.; Zhou, S.; Sun, C.; Yan, J.; Chen, P. Synthesis and Electromagnetic, Microwave Absorbing Properties of Core-Shell Fe_3O_4-Poly(3, 4-Ethylenedioxythiophene) Microspheres. *ACS Appl. Mater. Interfaces* **2011**, *3*, 3839−3845.
(42) Li, Z.; Zhang, J. T.; Guan, B. Y.; Wang, D.; Liu, L. M.; Lou, X. W. A Sulfur Host Based on Titanium monoxide@carbon Hollow Spheres for Advanced Lithium-Sulfur Batteries. *Nat. Commun.* **2016**, *7*, 13065.

https://doi.org/10.1021/acsomega.3c02138
ACS Omega 2023, 8, 23799−23805